α_v Integrins regulate germinal center B cell responses through noncanonical autophagy

Fiona Raso,[1] Sara Sagadiev,[1] Samuel Du,[2] Emily Gage,[3,4] Tanvi Arkatkar,[2] Genita Metzler,[2] Lynda M. Stuart,[1,5] Mark T. Orr,[3,4] David J. Rawlings,[2,6] Shaun W. Jackson,[2] Adam Lacy-Hulbert,[1,6] and Mridu Acharya[1]

[1]Immunology Program, Benaroya Research Institute at Virginia Mason, Seattle, Washington, USA. [2]Seattle Children's Research Institute, Seattle, Washington, USA. [3]Infectious Disease Research Institute, Seattle, Washington, USA. [4]Department of Global Health, University of Washington, Seattle, Washington, USA. [5]Bill and Melinda Gates Foundation, Seattle, Washington, USA. [6]Department of Immunology, University of Washington, Seattle, Washington, USA.

Germinal centers (GCs) are major sites of clonal B cell expansion and generation of long-lived, high-affinity antibody responses to pathogens. Signaling through TLRs on B cells promotes many aspects of GC B cell responses, including affinity maturation, class switching, and differentiation into long-lived memory and plasma cells. A major challenge for effective vaccination is identifying strategies to specifically promote GC B cell responses. Here, we have identified a mechanism of regulation of GC B cell TLR signaling, mediated by α_v integrins and noncanonical autophagy. Using B cell–specific α_v-KO mice, we show that loss of α_v-mediated TLR regulation increased GC B cell expansion, somatic hypermutation, class switching, and generation of long-lived plasma cells after immunization with virus-like particles (VLPs) or antigens associated with TLR ligand adjuvants. Furthermore, targeting α_v-mediated regulation increased the magnitude and breadth of antibody responses to influenza virus vaccination. These data therefore identify a mechanism of regulation of GC B cells that can be targeted to enhance antibody responses to vaccination.

Introduction

Strong B cell responses are a central component of effective long-lasting immunity to pathogens. B cells possess the unique ability to adapt the sequence of their immune receptors during the course of infection, allowing production of antibodies of increasing affinity to specific epitopes and greater breadth of binding to similar antigens. In addition, the generation of long-lived plasma and memory B cells allows rapid production of antibodies after subsequent encounters with the same or related pathogens. The generation of these durable, high-affinity antibody responses occurs predominantly in germinal centers (GC) in lymphoid organs and tissues. Here, B cells undergo multiple rounds of antigen-driven proliferation, somatic hypermutation (SHM) of immunoglobulin variable (V) regions, and selection to identify and expand cells expressing high-affinity antibodies (1, 2) and also undergo class switching and differentiation into plasma or memory cells. The formation and evolution of GCs during an immune response is therefore central in determining the durability, affinity, and diversity of antibodies.

Although the B cell receptor (BCR) is critical for the initial selection of antigen-specific B cells into the GC and for capture of antigen during affinity maturation, it is becoming increasingly clear that additional receptors on B cells determine the strength and outcome of GC reactions. Most notably, several studies have identified a critical role for TLRs in promoting strong GC responses (3–5). It has long been known that TLR ligands can be used as effective vaccine adjuvants and can induce outstanding immune responses (5). This property was originally attributed to TLRs on DCs, but recent studies have demonstrated that TLR signaling in B cells is also required for effective antibody responses. These studies indicate that TLR signaling in these 2 cell types performs distinct functions; whereas TLR signaling in DCs determines the magnitude of the GC reaction and the overall levels of antibody produced after vaccination, B cell TLR signaling promotes affinity maturation, class switching, and generation of memory B cells (6). Furthermore, the contribution of B cell TLR signaling to antibody responses is most pronounced when the antigen and TLR ligands are closely associated or covalently linked, consistent with a model in which coligation of BCR and TLR synergize for optimal activation of B cells. This model was originally proposed in the context of autoimmunity, where BCR recognition of nucleic acids or nuclear components promotes delivery of nucleic acids to endosomal TLR7 and TLR9, promoting activation of autoreactive cells (7–9). Thus, although TLR stimulation can promote effective B cell responses to pathogens, TLR engagement and signaling must also be regulated to prevent generation of high-affinity autoantibodies. The mechanisms by which this is achieved, and how this affects the balance between host defense and autoimmunity, remains poorly understood.

We have recently identified a new role for the vitronectin receptor $\alpha_v\beta_3$ integrin in the regulation of TLR signaling in marginal zone (MZ) and B-1 B cells (10). TLR signaling is tightly linked to

▶ Related Commentary: p. 3752

Conflict of interest: MA and ALH are named as inventors on a provisional patent (no. 62/591620) related to this work filed by Benaroya Research Institute.
Submitted: January 3, 2018; **Accepted:** June 26, 2018.
Reference information: *J Clin Invest*. 2018;128(9):4163–4178.
https://doi.org/10.1172/JCI99597.

subcellular localization, which controls access to ligands, and the availability of specific adaptor proteins, which dictate the outcome of TLR signaling (11). As an example, TLR4 signals through NF-κB when engaging ligands at the cell surface, but internalization of TLR4 ligand complexes to endosomes causes engagement of the adaptor TRIF and activation of IRF3 (12, 13). Likewise, endosomal TLRs, such as TLR7 and TLR9, initially activate NF-κB after engaging ligands and must traffic to a distinct endolysosomal compartment to signal though IRF7 (14). We showed that $\alpha_v\beta_3$ promotes the intracellular trafficking of TLRs to endosomes competent for IRF7 signaling and then to lysosomes, where TLR signaling is terminated. Deletion of either α_v or β_3 integrin subunits from B cells delays TLR trafficking, resulting in increased and prolonged TLR signaling through both NF-κB and IRF7 and increased B cell activation (10). $\alpha_v\beta_3$ Directs TLR trafficking by activation of components of the autophagy pathway, resulting in endosomal recruitment of the Atg8 family member microtubule-associated protein 1A/1B light chains 3B (LC3B). In this setting, LC3 does not form classical autophagosomes, but instead promotes TLR signaling through IRF7 and subsequently directs endosomal fusion with lysosomes. Hence, this appears to represent a form of noncanonical autophagy, analogous to the LC3-associated phagocytosis (LAP) described in macrophages and DCs (15). We have shown that $\alpha_v\beta_3$-mediated LC3 recruitment regulates the expansion of autoreactive MZ and B-1 B cells and that α_v-CD19 mice have increased titers of natural antibodies and autoantibodies to dsDNA. However, it is unclear whether this regulatory mechanism is specific to innate-like autoreactive B cell populations, such as MZ B cells, or also functions in classical B cell responses to complex foreign antigens.

Here, we report that α_v integrins play a major role in regulating GC B cell responses to foreign antigens and pathogens associated with TLR ligands and show that deletion of α_v from B cells greatly enhances the generation of high-affinity, long-lived B cell responses through specific effects on TLR signaling in GC B cells. TLR signaling in GC B cells activates lipidation of LC3 and relocalization to lysosomes through an α_v-dependent mechanism. Disruption of this process leads to increased TLR signaling and expansion of GC, memory, and plasma cells and promotes class switching and SHM. More importantly, our data indicate that loss of this pathway can enhance long-lived antibody responses to influenza virus. Thus, this study identifies a new role for α_v integrins and autophagy components in GC B cells and demonstrates that release of a regulatory mechanism previously associated with limiting autoimmunity can be beneficial in enhancing effective antibody responses to viruses.

Results

Deletion of α_v integrins from B cells causes increased GC B cell numbers. To determine whether $\alpha_v\beta_3$ regulates GC B cell responses, we first investigated GCs that arise spontaneously in the intestine. GC B cells isolated from Peyer's patches (PP) expressed both α_v and β_3 heterodimers, and surface expression of $\alpha_v\beta_3$ was several times higher than in non-GC B cells from the same lymphoid tissue (Figure 1A), as previously reported by Wang et al. (16). Spontaneous GC formation in the PP is stimulated by TLR ligands derived from commensal bacteria, and GC B cells purified from PP respond to TLR stimulation by activation of NF-κB. In addition, TLR stimulation of GC B cells causes aggregation and relocalization of LC3, consistent with TLR-mediated activation of autophagy components and fusion of LC3-containing endosomes to lysosomes, as we have previously reported for MZ and B-1 B cells. α_v-KO PP GC B cells showed increased and prolonged NF-κB activation in response to TLR stimulation (Figure 1B) and failed to reorganize LC3 (Figure 1, C and D). Deletion of α_v from B cells using the CD19-Cre knockin mouse strain (*Itgav$^{fl/fl}$; Cd19$^{Cre/+}$* mice, referred to as α_v-CD19 mice) resulted in an increase in GC B cell frequency in both PP and colon lamina propria compared with that in littermate control mice (*Itgav$^{fl/+}$; Cd19$^{Cre/+}$* genotype) (Figure 1, E and F). Together, these data show that GC B cells also mobilize the autophagy component LC3 after TLR stimulation through a mechanism involving α_v integrin and that deletion of α_v results in dysregulated TLR signaling and GC B cell expansion in vivo.

Increased GC B cells in α_v-CD19 mice immunized with TLR ligands. To study the role of α_v in GC cells in more detail, we immunized α_v-CD19 mice and littermate controls with virus-like particles (VLPs) derived from bacteriophage Qβ capsid proteins (17). These Qβ VLPs induce strong GC reactions that are dependent on B cell TLR7 signaling in response to ssRNAs contained within the VLP (17, 18). We first measured expansion of VLP-specific GC B cells, making use of fluorescent Qβ-VLPs. VLP$^+$ B cells were present at a very low frequency in nonimmunized mice, but could be readily detected in spleen and peritoneal-draining LNs after immunization (Figure 2A). VLP$^+$ B cells were present at a higher frequency in LNs from α_v-CD19 mice than in those from littermate controls after immunization. Furthermore, a higher proportion of VLP$^+$ B cells expressed GC markers (PNA$^+$, FAS$^+$, GL7$^+$) compared with those from control mice (Figure 2, B and C). A similar increase in VLP$^+$ GC cells was observed in the spleen of α_v-CD19 mice, although the overall frequency of VLP$^+$ B cells was not affected (Figure 2C). We reasoned that the increase in GC cells could be due to either increased recruitment to the GC pool or increased proliferation once in the GC, and to distinguish these possibilities, we measured GC B cell proliferation by incorporation of the nucleoside analog BrdU. A higher proportion of BrdU$^+$ VLP-specific B cells was seen in α_v-CD19 mice than in controls (Figure 2D), suggesting that increased proliferation was responsible for the higher numbers of GC B cells in α_v-CD19 mice. GC B cell proliferation and expansion occur primarily in the dark zone (DZ), and we also observed an increase in VLP-specific cells expressing markers consistent with GC DZ occupancy in α_v-CD19 mice (Figure 2E), further supporting this explanation.

Loss of α_v confers a competitive advantage to GC cells. To test whether the effects of α_v deletion on GC B cell proliferation were cell intrinsic, we generated mixed BM chimeras between α_v-CD19 and WT congenic mice (B6.SJL) (at 1:1 ratio; Figure 3A). Chimeras were immunized with VLPs and relative numbers of α_v-deficient and congenic cells in B cell compartments measured (Figure 3B). The relative proportion of α_v-deficient B cells in the total B cell population was similar to that in other hematopoietic cells, indicating that α_v deletion did not greatly affect differentiation into B cells. However, the proportion of α_v-deficient B cells in the VLP$^+$ population was significantly higher than in the total B cell pool and was further increased in the VLP$^+$ GC population, where in some cases over 90% of VLP$^+$ GC cells were derived from α_v-deficient

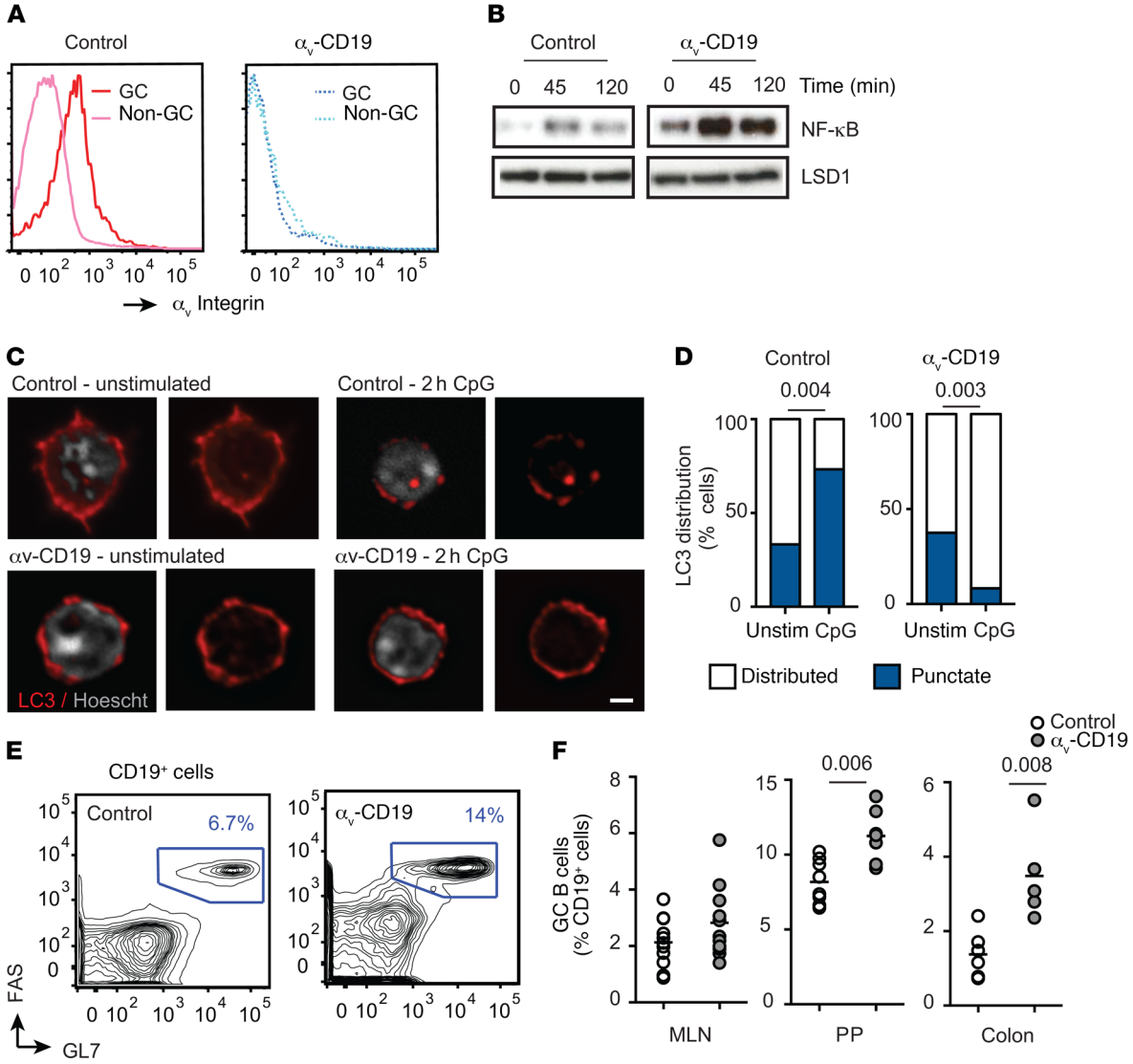

Figure 1. Increased GC B cells in α_v-CD19 mice. (**A**) Histograms show staining for α_v on CD19⁺ cells from control mice (solid lines) or α_v-CD19 mice (dotted lines). (**B**) Western blot analysis of NF-κB p65 in nuclear fractions from FACS-sorted PP GC cells from control and α_v-CD19 mice stimulated in vitro with CpG for the indicated times (minutes). Also shown is the staining for LSD1 to confirm equal loading of nuclear protein. (**C**) Confocal microscopy of FACS-sorted PP GC B cells from control and α_v-CD19 mice with or without in vitro stimulation with 2 μM CpG DNA for 2 hours. Cells are stained for LC3b (red) or nuclear DNA (Hoescht, white). Images show representative examples of distributed LC3 expression (unstimulated control and α_v-CD19) and punctate expression (CpG-treated control). Scale bar: 2.5 μm. (**D**) Proportions of cells undergoing LC3 reorganization, based on counting of at least 30 cells/condition. *P* values are shown (Pearson's χ^2 test). (**E**) Representative FACS plots of cells from PP of control and α_v-CD19 mice gated on CD19⁺ B cells and stained with FAS/GL7. Gates used for identification of GC B cells and frequency of GC B cells are shown. (**F**) Quantification of frequency of GC B cells in mesenteric lymph nodes (MLN), PP, and colon lamina propria in control and α_v-CD19 mice. GC B cells were gated as CD19⁺GL7⁺FAS⁺ cells as in **E**. Each point represents an individual mouse, and at least 5 mice were analyzed for each group. *P* values of less than 0.05 are shown (2- tailed Student's *t* test). For all data shown, similar results were seen in at least 3 independent experiment.

BM (Figure 3C). Selection into the VLP⁺ and GC pools was not seen in equivalent chimeras between control cells (which carry the same CD19-Cre allele as those from α_v-CD19 mice) and WT congenic cells (Con-WT) (Figure 3, B and C). Based on these data, we concluded that deletion of α_v provides a competitive advantage to GC B cells and that expansion of GC B cells in α_v-CD19 mice was due to cell-intrinsic effects of α_v deletion on GC B cells.

α_v Integrins activate autophagy components and regulate TLR signaling in GC B cells. To determine whether α_v directly affects GC B cell responses to stimulation, GC B cells from VLP-immunized control and α_v-CD19 mice were purified and restimulated in vitro. Stimulation of purified GC B cells with either VLPs or the TLR9 agonist CpG DNA induced rapid activation of NF-κB (by 45 minutes), which was transient, declining to close to baseline levels by 120 minutes (Figure 4A). Stimulation of GC B cells also resulted in activation of IRF7, which occurred with slightly slower kinetics than NF-κB, remaining elevated 120 minutes after stimulation with VLPs (Figure 4A). Similar to our previous findings in MZ B cells (10), TLR stimulation of GC B cells triggered lipidation of the autophagy component LC3 (Figure 4B) and reorganization of LC3

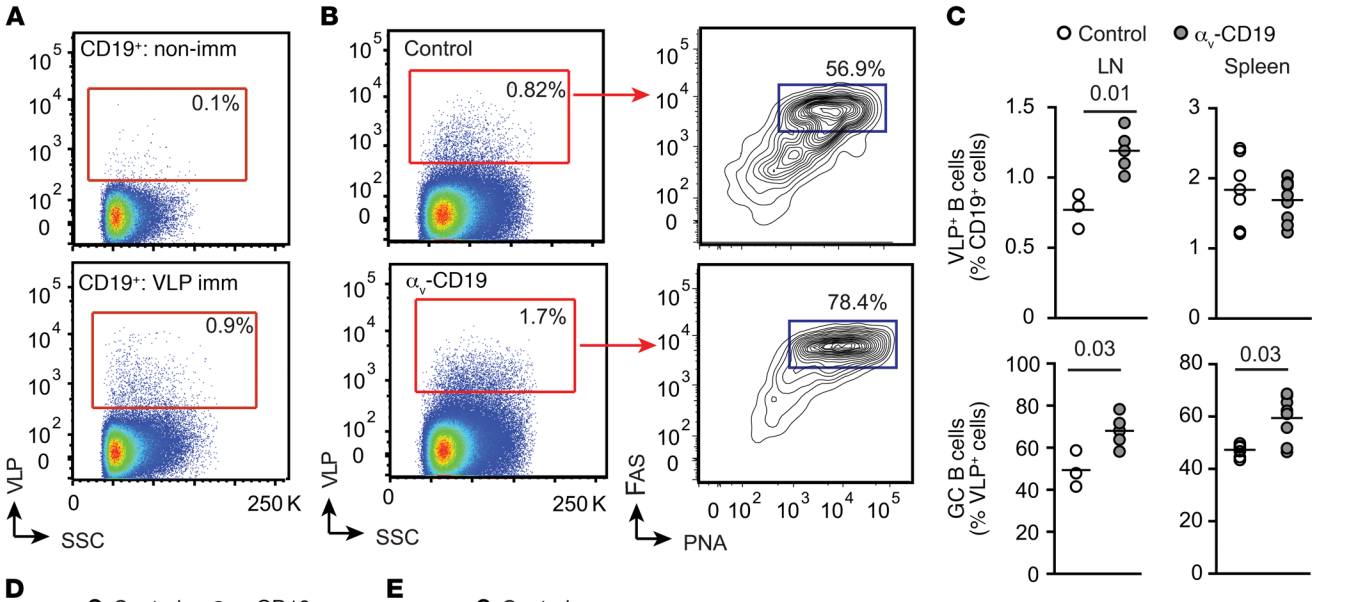

Figure 2. Increased GC B cells in α_v-CD19 mice immunized with TLR ligands. (**A**) FACS plots of cells from LNs from VLP-immunized and nonimmunized (non-imm) mice stained with fluorescent VLPs, showing VLP$^+$ cells in CD19$^+$ gate. Gating strategy for VLP-specific B cells based on nonimmunized mice is shown. SSC, side scatter. (**B**) Representative FACS analysis of VLP$^+$ cells from mediastinal and abdominal LNs of control and α_v-CD19 mice 14 days after immunization with 2 μg VLPs. Left panels show on CD19$^+$ cells and gates used to identify VLP$^+$ cells. Right panels show GC B cells (PNA$^+$FAS$^+$ cells) within the CD19$^+$VLP$^+$ gate. (**C**) Quantification of VLP$^+$ cells and VLP$^+$ GC cells in VLP-immunized control and α_v-CD19 mice. Each point represents a single mouse; bars show mean. (**D**) Proportion of LN and spleen VLP$^+$ GC B cells (gated as in **B**) from control and α_v-CD19 mice immunized with 2 μg VLP for 14 days that stain positive for BrdU 12 hours after BrdU administration. (**E**) VLP-specific GC cells were gated based on expression of markers of DZ (CXCR4$^+$CD86^{lo}) and light zone (LZ) (CD86$^+$CXCR4^{lo}). Data show ratio of DZ/light zone cells in individual mice. Bars show the mean. In all cases, *P* values of less than 0.05 are shown (Mann-Whitney-Wilcoxon test). For all data shown, similar results were seen in at least 3 independent experiments.

from a distributed pattern throughout the cytosol to aggregates at the center of the cell (Figure 4, C and D). We have previously shown that these aggregates correspond to LAMP2$^+$ lysosomes (10). Consistent with a role for LC3 in lysosomal trafficking, levels of the cargo receptor p62, which binds LC3 and is degraded after lysosomal fusion, dropped sharply in control GC B cells following TLR stimulation (Figure 4B). In α_v-deficient GC B cells, NF-κB signaling was increased and prolonged in response to TLR or VLP stimulation, remaining highly elevated 2 hours after stimulation, while IRF7 activation was delayed (Figure 4A). α_v-KO GC B cells also did not show increases in LC3 lipidation (Figure 4B and Supplemental Figure 1; supplemental material available online with this article; https://doi.org/10.1172/JCI99597DS1) and reorganization (Figure 4C) or p62 degradation (Figure 4B and Supplemental Figure 1). Hence, we concluded that α_v regulates TLR signaling in GC B cells and that this occurs through the autophagy-related mechanism.

Curiously, although non-GC follicular B cells from VLP-immunized mice also respond to stimulation with VLPs and TLR9 agonists, as evidenced by NF-κB activation, they did not show any detectable activation of IRF7 or increase in LC3 lipidation, LC3 reorganization, or degradation of p62 (Figure 4, E and F, and Supplemental Figure 2). Indeed, non-GC follicular cells expressed much lower levels of LC3 and p62 than GC cells from the same mouse (Figure 4, B and F). Furthermore, we did not observe any significant difference between TLR responses in α_v-KO and control non-GC follicular B cells. Based on these results, we conclude that the ability of α_v to activate autophagy components following TLR signaling is a specialized property acquired by GC B cells and that this allows activation of IRF7 in response to TLR ligands, but also regulates the strength and duration of TLR signaling in these cells.

To determine how α_v deletion and altered TLR signaling affect the activation and expansion of B cells in GCs, we examined expression of key genes involved in GC B cell function and differentiation. Expression of genes involved in SHM (*Aicda* or AID), plasma cell differentiation (*Prdm1*/BLIMP), and class switching to IgG2c (*Tbx21*/T-bet) were all increased in VLP$^+$ GC cells from α_v-CD19 mice compared with control cells, whereas genes involved in general GC differentiation (*Myc* and *Bcl6*) were either unchanged or downregulated (Figure 4G). Furthermore, these changes in gene expression were observed as early as day 5 after immunization and sustained at 14 days. Together, these data show that increased GC B cell expansion in α_v-CD19 mice is associated with stronger responses to TLR stimulation and leads to qualitative differences in GC B cell phenotype.

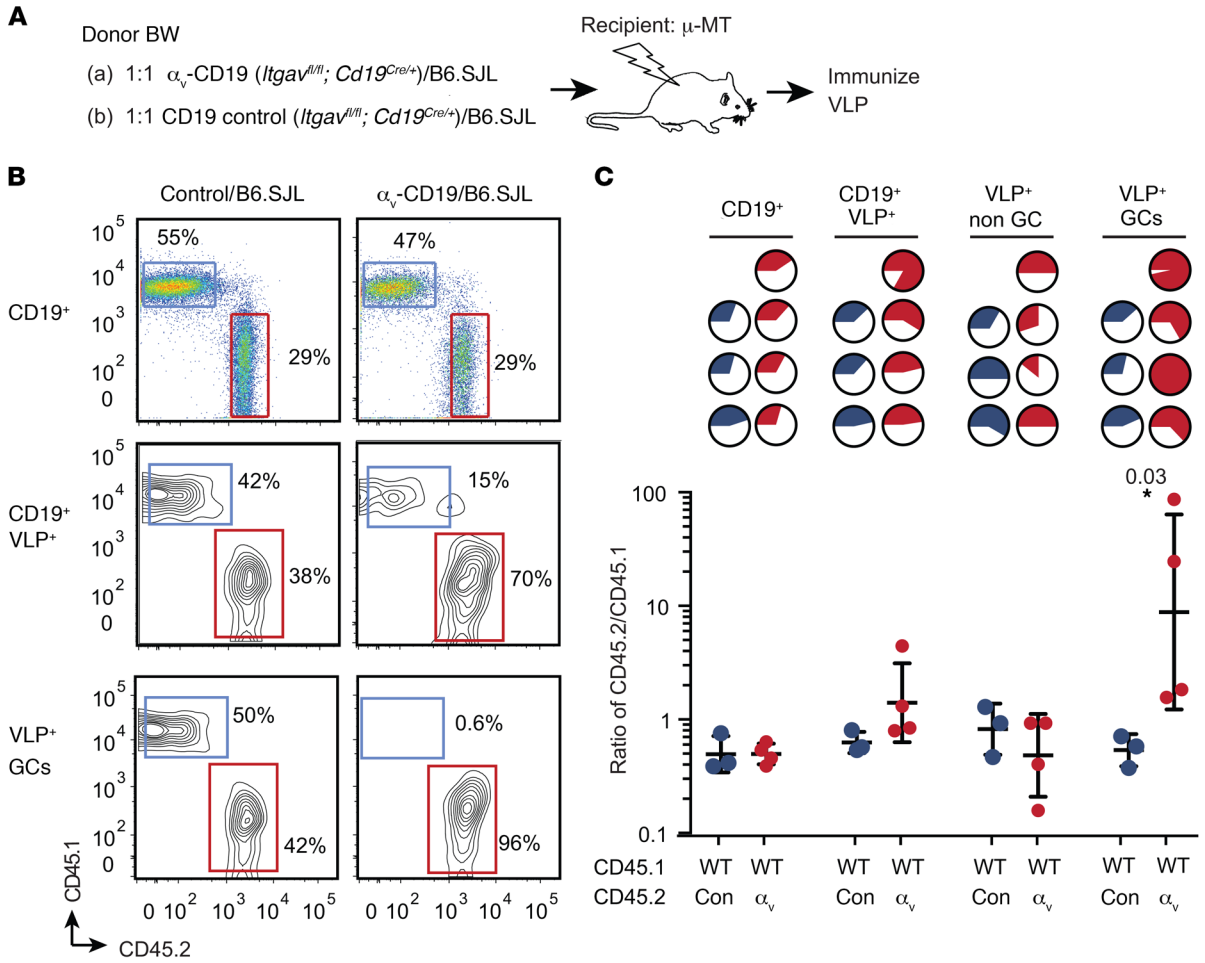

Figure 3. Loss of α_v confers competitive advantage to GC cells. (**A**) Schematic for the experimental plan. CD138-depleted BM cells from congenically marked CD45.1 mice (B6.SJL) were mixed at a 1:1 ratio with BM cells from CD45.2 α_v-CD19 mice and injected into irradiated μ-MT mice to generate mixed BM chimeras. Control chimeras were generated with a 1:1 mix of B6.SJL BM and CD45.2 control CD19-Cre BM cells. Six weeks after reconstitution, mice were immunized with 2 μg VLP and harvested at day 14 for analysis of antigen-specific B cells by FACS. (**B**) Representative FACS panels for analysis of composition of CD45.1 and CD45.2 cells in CD19$^+$, CD19$^+$VLP$^+$, or CD19$^+$VLP$^+$ GC B cell compartments. GC cells were identified as PNA$^+$FAS$^+$ cells. (**C**) Pie charts in top section of panel show relative proportions of CD45.2$^+$ cells (solid regions of pie charts) in control chimeras (blue) and α_v-CD19 chimeras (red) in indicated B cell compartments; each pie chart represents 1 mouse. Lower panel shows data from all mice in each group expressed as ratio of CD45.2/CD45.1 and geometric mean ± SD. Ratios of CD45.2/CD45.1 cells for VLP$^+$ non-GC and GC B cells from WT/α_v chimeras were compared by 2-tailed Student's *t* test of log-transformed data. *P* value is shown. Data are from 1 representative experiment, with similar results seen in 3 independent experiments.

Noncanonical autophagy regulates GC B cell response. To specifically address the role of noncanonical autophagy in GC response, we focused on Rubicon, a protein that has recently been described as required for LAP, a form of noncanonical autophagy, but that is not required for macroautophagy (19). We confirmed that Rubicon was also required for TLR-induced autophagy in B cells, as LC3 lipidation was impaired in MZ B cells from Rubicon-KO mice after stimulation with the TLR9 agonist CpG (Figure 5A). Furthermore, B cells from Rubicon-KO mice showed increased proliferation in response to TLR9 and TLR7 ligands (Figure 5, B and C) compared with control cells, which was similar to our previous findings with α_v-deficient, Atg5-deficient, and LC3-deficient B1 and MZ B cells (10). This effect was not seen in follicular B cells, and loss of Rubicon did not enhance B cell responses to IgM stimulation (Figure 5D), demonstrating that, as with α_v-deletion, the effects of noncanonical autophagy were specific to stimulation of activated B cell populations by TLR ligands.

To directly address the role of Rubicon in GC B cells,we used a competitive assay, as outlined in Figure 3. Mixed BM chimeras generated with a 1:1 ratio of Rubicon-KO and WT congenic cells were immunized with VLP, and proportions of KO cells in the VLP-reactive GC and non-GC subsets assessed by FACS. Rubicon-deficient B cells were significantly enriched in the VLP$^+$ GC compartment (Figure 5E), indicating that loss of Rubicon provides a competitive advantage to GC B cells, as we have seen with α_v-deficient cells. Together, these data support our hypothesis that α_v regulates GC B cell responses through Rubicon-mediated noncanonical autophagy.

α_v-CD19 mice produce higher IgG2c titers in response to TLR ligand adjuvants. We next analyzed the effects of changes in GC B cells on antibody production in α_v-CD19 mice. Titers of serum anti-VLP IgG were increased by approximately 2-fold in α_v-CD19 mice compared with controls (Figure 6A) following immunization with VLPs. Similar increases were seen in anti-VLP IgG2c in α_v-

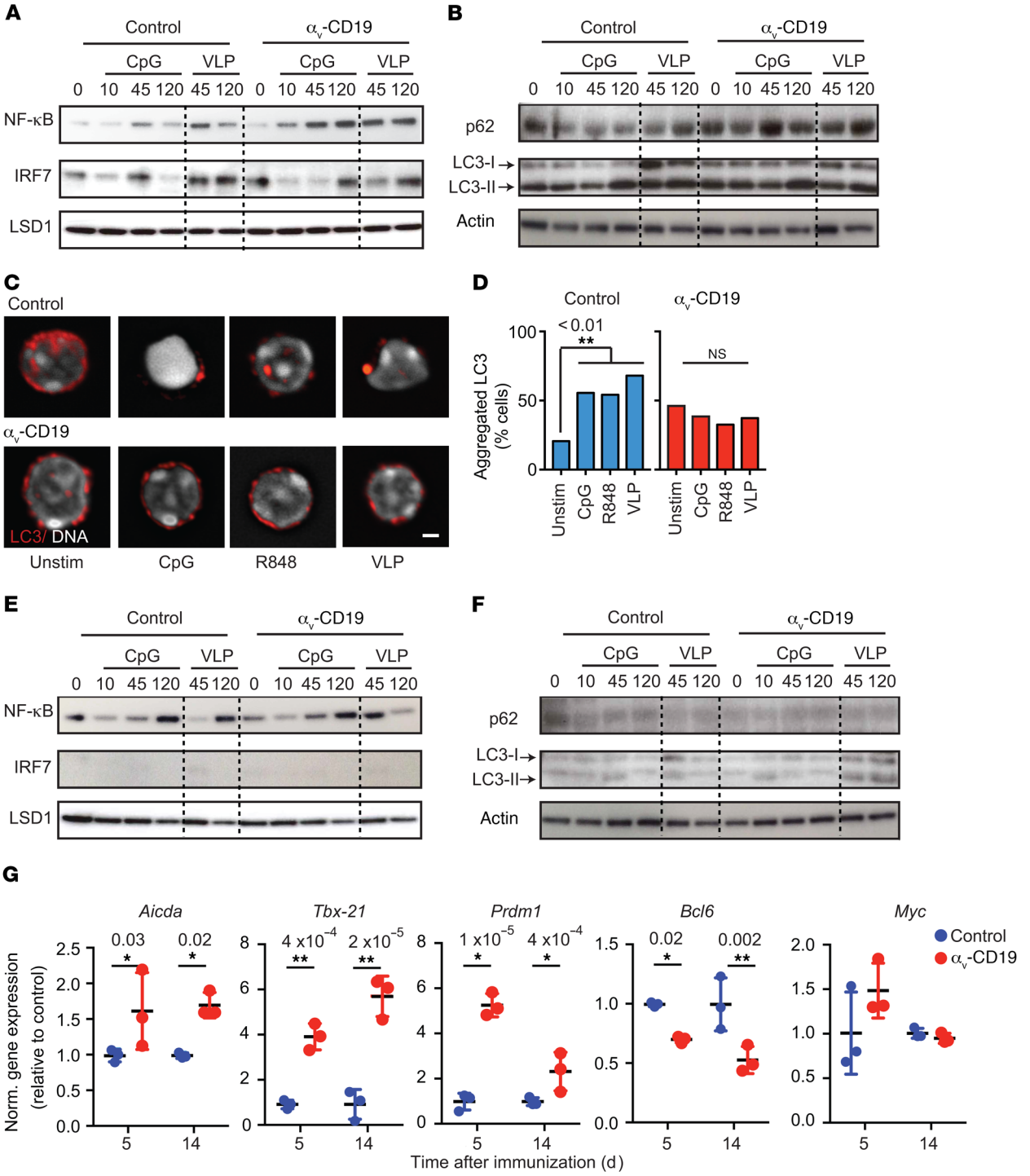

Figure 4. α_v Regulates TLR signaling in GC B cells through autophagy proteins. (**A** and **B**) GC B cells were sorted from spleens of α_v-CD19 and control mice 14 days after immunization with VLP and restimulated in vitro with CpG DNA or VLP for the indicated times (minutes). Western blots show NF-κB p65 and IRF7 in nuclear fractions (**A**) or p62 and LC3b in whole-cell lysates (**B**). Also shown is staining of LSD1 or actin to confirm equivalent protein loading in nuclear fraction and whole-cell lysates, respectively. These were performed on the same blot, except in the case of LC3-II, for which actin staining was from aliquots of the same samples run on parallel gels contemporaneously. (**C**) Confocal images of sorted primary GC B cells (as in **A** and **B**) treated with CpG DNA, R848, or VLP for 2 hours and stained for LC3 and Hoescht. Scale bar: 2.9 μm. (**D**) Quantification of LC3 reorganization after stimulation with indicated TLR ligands. Data are based on analysis of at least 30 cells/condition. *P* values of less than 0.01 are shown (Pearson's χ^2 test). $^*P < 0.05$. (**E** and **F**) FACS-sorted non-GC follicular B cells from spleens of VLP-immunized α_v-CD19 and control mice analyzed as in **A** and **B**. (**G**) Expression of indicated genes measured by quantitative reverse-transcriptase PCR (QRT-PCR) in RNA from FACS-sorted VLP-specific GC cells, isolated 5 or 14 days after immunization with 2 μg VLPs. Data from individual mice are shown, with mean ± SD. *P* values of less than 0.05 are shown (2-tailed Student's *t* test). $^*P < 0.05$; $^{**}P < 0.005$. Data are all from 1 representative experiment of at least 3 independent experiments (2 experiments for p62 blots) in which similar results were seen.

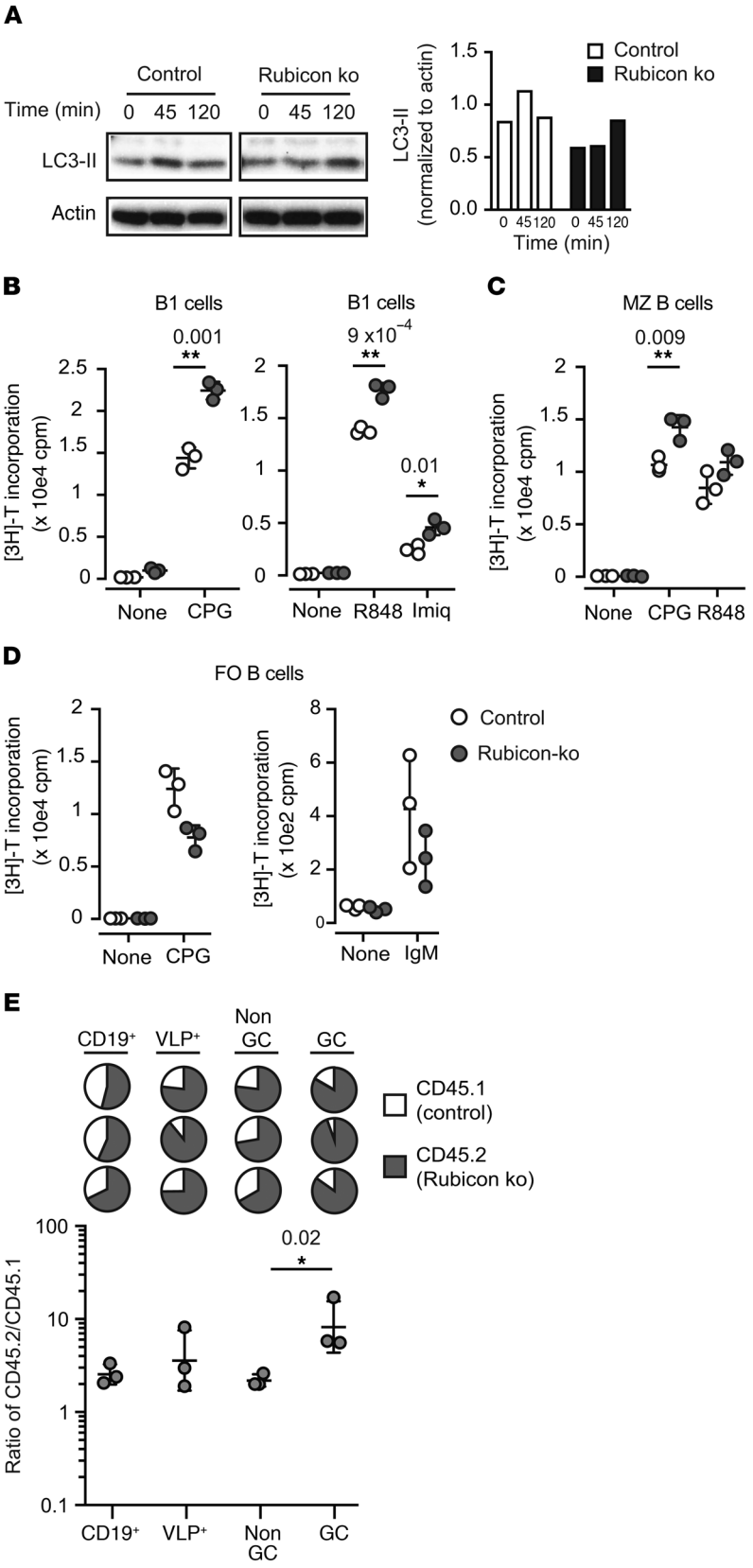

Figure 5. Rubicon-mediated noncanonical autophagy regulates B cell TLR responses. (**A**) MZ B cells from Rubicon-KO and control mice were stimulated in vitro with CpG DNA for the indicated times (minutes). Western blots show LC3b and actin in whole-cell lysates. Histogram shows quantification of LC3-II normalized to actin for this blot. Similar results were seen in 3 independent experiments. (**B**–**D**) Proliferation of peritoneal B1 B cells (**B**), sorted spleen MZ B cells (**C**), and spleen follicular (FO) B cells (**D**) from Rubicon-KO and control mice after stimulation with TLR ligands (CpG DNA, R848, and imiquimod) or anti-IgM. Proliferation was measured by [^{3}H]-thymidine incorporation and is expressed as mean ± SD for 3 independent cultures. *P* values of less than 0.05 are shown (2-tailed Student's *t* test). $^*P < 0.05$; $^{**}P < 0.01$. Similar results were seen in 3 independent experiments. (**E**) Mixed BM chimeras between control C57BL/6.SJL congenic mice and Rubicon-KO mice (CD45.2) were generated and used to assess competitive recruitment to the GC compartment as described in Figure 3. Pie charts show relative proportions of CD45.2$^+$ cells (solid regions) in indicated B cell compartments; each pie chart represents 1 mouse. Lower panel shows data from individual mice expressed as the ratio of CD45.2/CD45.1. Also shown are the geometric means ± SD. Ratios of CD45.2/CD45.1 cells for VLP$^+$ non-GC and GC B cells were compared by 2-tailed Student's *t* test of log-transformed data. *P* value is shown. Similar results were seen in 2 independent experiments.

CD19 mice, whereas anti-VLP IgG1 and IgM were not significantly different from in controls (Figure 6A). Anti-VLP IgG and IgG2c titers were increased in α_v-CD19 mice at day 14 and day 21 after immunization, but dropped to levels similar to those in control mice as the primary antibody response waned at day 35 and beyond, indicating that α_v-deletion affected the magnitude of the primary immune response, but not the duration (Figure 6B). Strong antibody responses to Qβ-VLPs have been shown to require TLR signaling in B cells and DCs, which is triggered by ssRNA contained within the VLP binding to TLR7. To confirm that increases in VLP antibody response in α_v-CD19 mice were due to effects on TLR signaling, mice were immunized with Qβ-VLPs lacking ssRNA. Both α_v-CD19 and control mice mounted antibody responses to these "empty" VLPs, but levels of anti-VLP IgG and IgG2c were significantly (5- to 10-fold) lower than in mice immunized with ssRNA-containing VLPs, whereas IgG1 titers were unchanged (Supplemental Figure 3), as reported previously (18). Importantly, we saw no difference in antibody titers between α_v-CD19 and control mice in response to TLR ligand–free VLPs, demonstrating that the differences in anti-VLP responses in α_v-CD19 mice were dependent on TLR signaling.

To determine whether the increases in IgG2c titers in α_v-CD19 mice could be explained solely by increased responses to TLR7 signaling, we

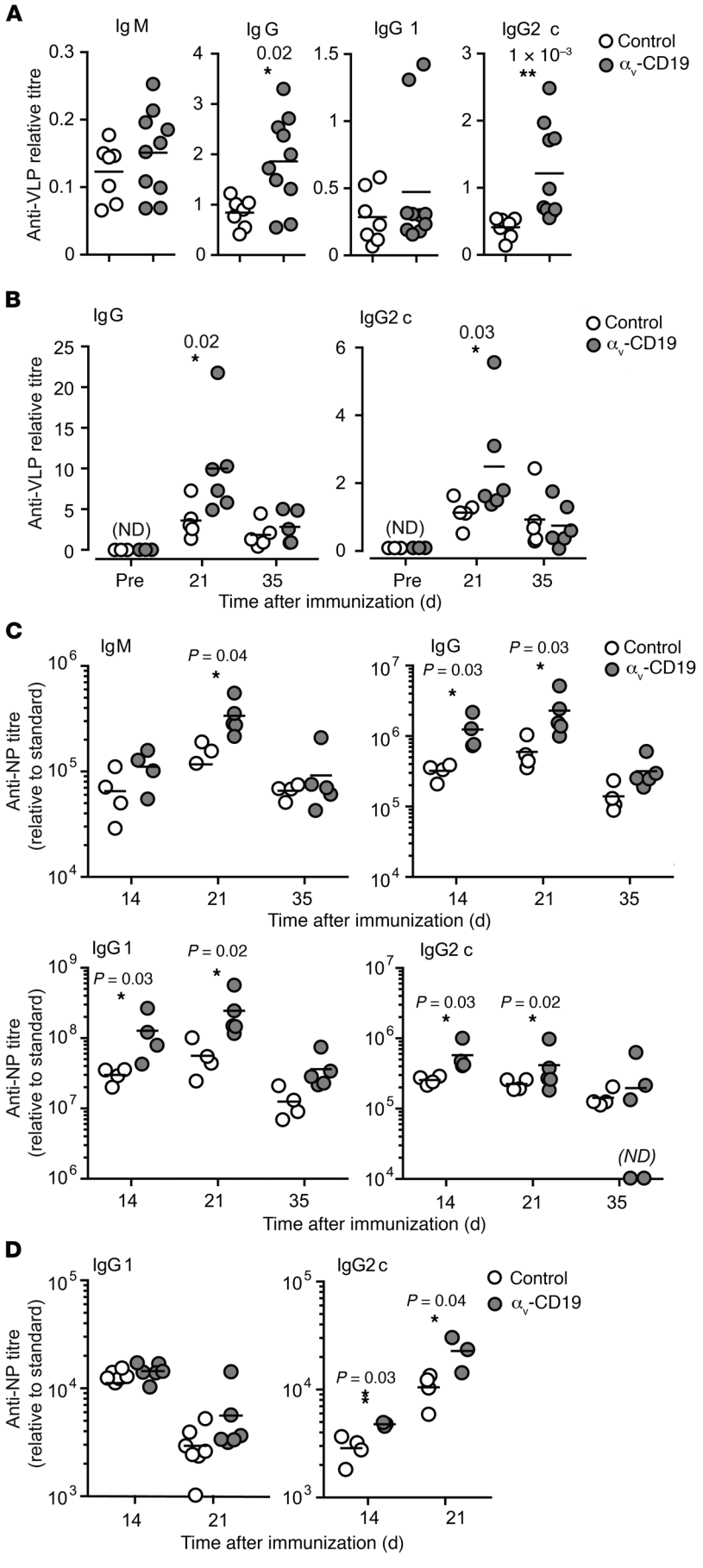

Figure 6. Increased antibody production in α_v-CD19 mice. (**A**–**B**) Serum anti-VLP antibody titers in control and α_v-CD19 mice immunized with 2 μg VLPs containing ssRNA measured 14 days after immunization (**A**) or over a time course from preimmunization (pre) to 35 days (**B**). VLP-specific Abs were not detected (ND) in preimmunization bleeds. (**C**) Serum anti-NP IgM, IgG, IgG1, and Ig2c titers in control and α_v-CD19 mice immunized with NP-CG (50 μg) combined with TLR7 ligand imiquimod-SE (10 μg). (**D**) Serum anti-NP IgG1 and IgG2c antibody titers in control and α_v-CD19 mice immunized with NP-CG (50 μg) combined with LPS (5 μg). All data points represent individual mice with mean shown. *P* values of less than 0.05 are shown (Mann-Whitney-Wilcoxon test). $*P < 0.05$; $**P < 0.005$. Samples below the level of detection are indicated as not detected. Similar results were seen in 3 independent experiments.

substituted VLPs for a vaccine-grade formulation of the TLR7 agonist imiquimod (imiquimod-SE), combined with a model protein antigen, nitrophenol-haptenated chicken γ-globulin (NP-CG). Similarly to our findings with VLP immunization, α_v-CD19 mice immunized with NP-CG/imiquimod-SE produced higher serum titers of anti-NP IgG2c than control mice (Figure 6C). In addition, α_v-CD19 mice also produced higher levels of anti-NP IgM and IgG1 than control mice, although these increases were less pronounced than for IgG2c. In our previous study, we showed that α_v-CD19 mice produced normal levels of IgG1 and IgG2c in response to NP-CG in the presence of an alternative, TLR-independent adjuvant, alum, but IgG2c levels were elevated when the TLR4 ligand LPS was used as an adjuvant (ref. 10 and Figure 6D). Together, these data show that the α_v-CD19 mice mount stronger primary IgG2c antibody responses to antigens associated with either endosomal (TLR7) or cell-surface (TLR4) TLRs, supporting our hypothesis that changes in GC B cell function and increased antibody responses in α_v-CD19 mice are due to loss of regulation of TLR signaling.

α_v Regulates long-lived antibody responses to TLR ligand adjuvants. A hallmark of GC reactions is the generation of long-lived plasma cells and memory cells that provide long-term immunity and rapid antibody responses to previously encountered pathogens. To determine whether α_v integrins affected either of these aspects of the immune response, VLP-immunized mice were rechallenged with low doses of VLPs. To focus on reactivation of B cells by antigen alone and avoid complications from any increased TLR signaling in α_v-deficient memory or plasma B cells, we used "empty" VLPs, lacking ssRNA, for secondary challenge. α_v-CD19 mice produced higher titers of anti-VLP IgG than controls 7 days after rechallenge (Figure 7A). As we had observed for primary responses, this increase in IgG was predominantly associated with increases

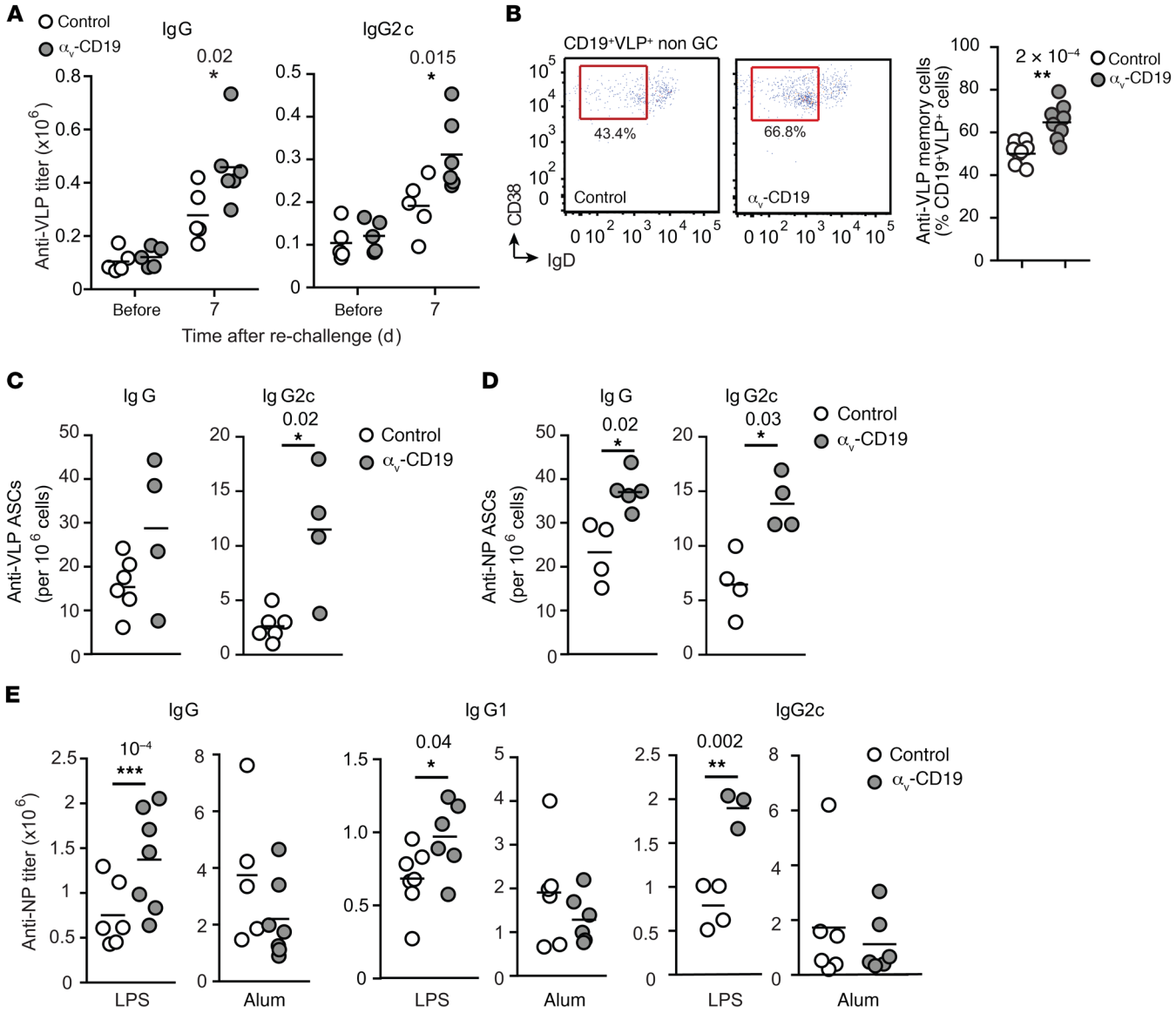

Figure 7. Loss of α_v affects long-lived antibody responses. (**A**) Serum anti-VLP IgG and IgG2c titers in control and α_v-CD19 mice immunized with 2 μg VLPs containing ssRNA that were boosted with empty VLP at day 68 and harvested after a further 7 days. (**B**) Frequency of VLP-specific CD38$^+$IgD^{lo} B cells in control and α_v-CD19 mice at day 7 after boost as in **A**. (**C** and **D**) Antigen-specific plasma cells enumerated by ELISpot assay on BM cells from control or α_v-CD19 mice harvested after immunization and rechallenged with either (**C**) VLPs (2 μg) or (**D**) NP-CG with imiquimod-SE. (**E**) Serum anti-NP IgG, IgG1, and IgG2c titers in control and α_v-CD19 mice immunized initially with NP-CG with either LPS or alum and boosted at day 42 with NP-CG (25 μg) alone. All data points represent individual mice with mean shown. *P* values of less than 0.05 are shown (Mann-Whitney-Wilcoxon test). $^*P < 0.05$; $^{**}P < 0.005$. Similar results were seen in 3 independent experiments.

in IgG2c (Figure 7A), while anti-VLP IgG1 levels were similar in the 2 strains (not shown). Memory B cells reside in the spleen and other lymphoid organs and expand in response to reexposure to antigen to generate plasma cells or reenter GC reactions. VLP-specific memory B cells, identified on the basis of VLP, CD38, and IgD staining, were present at a higher frequency in the spleens of rechallenged α_v-CD19 mice than in controls (Figure 7B). Long-lived plasma cells in the BM constitutively produce large amounts of antibody. Consistent with the higher levels of serum anti-VLP antibody, we observed greater numbers of VLP-specific IgG2c antibody–producing cells in the BM of rechallenged α_v-CD19 mice than in equivalent control mice (Figure 7C). To confirm that these increased memory responses in α_v-CD19 mice required TLR signaling, we again made use of the model antigen NP-CG, with either TLR ligand (imiquimod-SE and LPS) or TLR-independent (alum) adjuvants. α_v-CD19 mice immunized with NP-CG in the presence of TLR ligand adjuvants and rechallenged with NP-CG alone had higher numbers of BM anti-NP antibody-producing cells and higher serum titers of anti-NP IgG antibody (Figure 7, D and E). In contrast, memory responses in α_v-CD19 mice immunized with NP-CG in alum adjuvant were no different from those in controls (Figure 7E). Hence, loss of α_v-mediated regulation

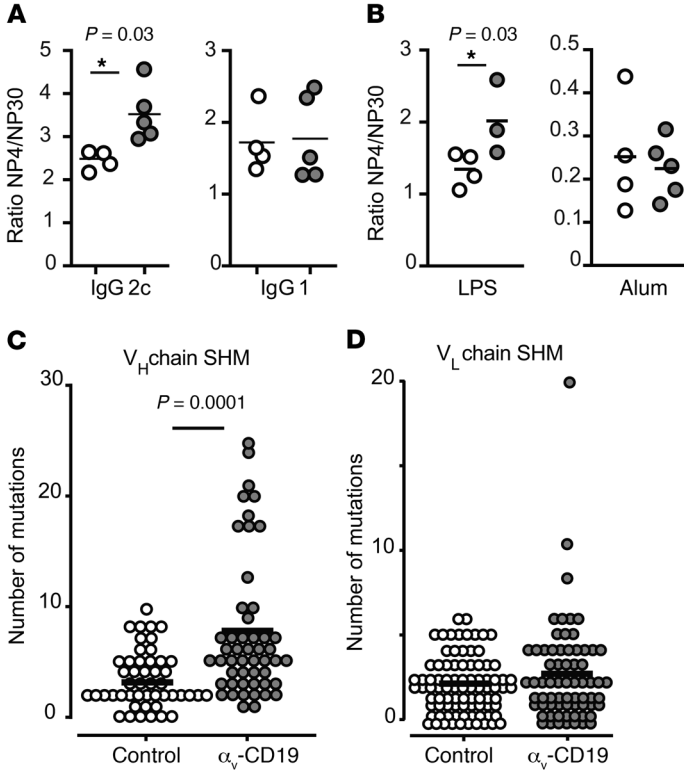

Figure 8. Deletion of α_v promotes SHM and affinity maturation of antibodies. (**A** and **B**) Affinity maturation of antibodies measured as ratio of anti-NP4/anti-NP30 titers in serum of NP-CG–immunized mice rechallenged with NP-CG at day 42 and bled after a further 7 days. Mice were initially immunized with NP-CG and imiquimod-SE (**A**) or NP-CG in LPS or alum (**B**). Data points represent individual mice with mean shown. *P* values of less than 0.05 are shown (Mann-Whitney-Wilcoxon test). $^*P < 0.05$. Similar results were seen in 3 independent experiments. (**C** and **D**) Point mutations in the IgG heavy chain (V_H) (**C**) or light chain (V_L) (**D**) of individual spleen VLP$^+$ GC B cells 14 days after immunization with 2 μg VLPs. Each dot indicates a single cell, and line indicates the mean. Mutations were identified by comparing with germline sequences. *P* values of less than 0.05 are shown (Mann-Whitney-Wilcoxon test).

of TLR signaling affects the generation of memory and plasma cells, consistent with the expansion of GC B cells and increased expression of genes associated with plasma cell differentiation in α_v-CD19 mice.

Deletion of α_v promotes SHM and high-affinity antibody responses. A second critical function of GC reactions is to provide antibody diversity and select high-affinity antibodies through successive rounds of immunoglobulin mutation and selection. The affinity of polyclonal serum antibodies to the hapten NP can be assessed by ELISA using NP_{30}- and NP_4-conjugated BSA to measure total and high-affinity Igs, respectively. The ratio of serum IgG2c measured using NP_4 versus NP_{30} (i.e., the ratio of high- to low-affinity antibody) was significantly higher in NP-CG/imiquimod-SE–immunized α_v-CD19 mice than in littermate controls (Figure 8A). Similar increases in Ig affinity were seen in mice immunized with NP-CG combined with a different TLR adjuvant, LPS, but not in mice immunized with NP-CG in alum (Figure 8B). Notably, increased affinity was only seen for the IgG2c isotype and not for IgG1, consistent with the ability of TLR signaling to promote both affinity maturation and IgG2c class switching and the role of AID in both processes. The increased high-affinity antibodies, expansion of GC B cells, and expression of higher levels of AID (*Aicd* gene) in α_v-CD19 mice suggested that α_v-KO GC cells undergo increased SHM compared with controls. To test this hypothesis, VLP$^+$ GC cells were sorted from α_v-CD19 and control mice 14 days after immunization, and BCR heavy and light chains from individual cells were sequenced (20). V_H and V_L sequences were generated from between 49 to 87 single cells and matched to reference genomic sequences; the number and position of mutations were then determined. α_v-CD19 mice showed a significant increase in mutations in IgG_H compared with littermate control mice (Figure 8, C and D).

Deletion of α_v enhances antibody response to influenza virus. Effective vaccination against many viruses relies on the generation of long-lived high-affinity neutralizing antibodies. To examine the effects of increased GC responses in α_v-CD19 mice on antibody response to viruses, mice were immunized with inactivated influenza A/PR/8/34 virus (PR/8). α_v-CD19 mice produced up to 3-fold greater titers of anti-PR/8 IgG antibodies than littermate control mice (Figure 9A). Antibody titers remained elevated over control mice at 56 days after immunization, and after a second immunization, titers were further increased in α_v-CD19 mice compared with controls (Figure 9B). Furthermore, as seen in our VLP and TLR ligand adjuvant immunization studies, α_v-CD19 mice generated higher numbers of BM anti-PR/8 antibody–producing plasma cells than controls (Figure 9C), indicating that deletion of α_v promotes increased long-lived antibody responses against influenza virus.

A major target of antibody responses to influenza virus is the viral HA. To determine whether the increased antibodies produced in α_v-CD19 mice were functional and effective against influenza, serum from mice at day 21 after immunization was tested for hemagglutination inhibition (HAI) activity. Serum from α_v-CD19 mice had 4-fold higher HAI than serum from littermate control mice (Figure 9D). This correlated with increased titers of IgG antibodies against PR/8 in α_v-CD19 mice, and as we had seen for VLPs and TLR ligand–associated antigens, this increase in anti-HA IgG was predominantly due to increases in IgG2c antibody (Figure 9E). HA is a major source of antigenic variation in influenza, and accumulation of mutations in antibodies during GC reactions has been shown to broaden their reactivity to different influenza HA epitopes (21). To assess whether increased GC responses in α_v-CD19 mice were capable of generating antibodies of broader reactivity, we measured the binding of serum from PR/8-immunized mice to HA from the 2009 pandemic H1N1 strain, influenza A California/04/2009 (Cal/09). Serum from all α_v-CD19 mice tested recognized Cal/09 HA, whereas this was only seen for 1 control mouse (of 3) (Figure 9F). This increase in Cal/09 HA binding remained after normalization to PR/8-HA binding for each sample (Figure 9G), suggesting that Cal/09-HA binding could not simply be explained by a higher level of anti-HA antibodies in α_v-CD19 mice. However, to overcome any confounding effects from the lower levels of antibody response in controls, mice were immunized with inactivated PR/8 in combination with a TLR ligand adjuvant, imiquimod-SE. Addition of imiquimod induced more uniform and robust anti-HA responses in control mice (Figure 9H). Furthermore, consistent

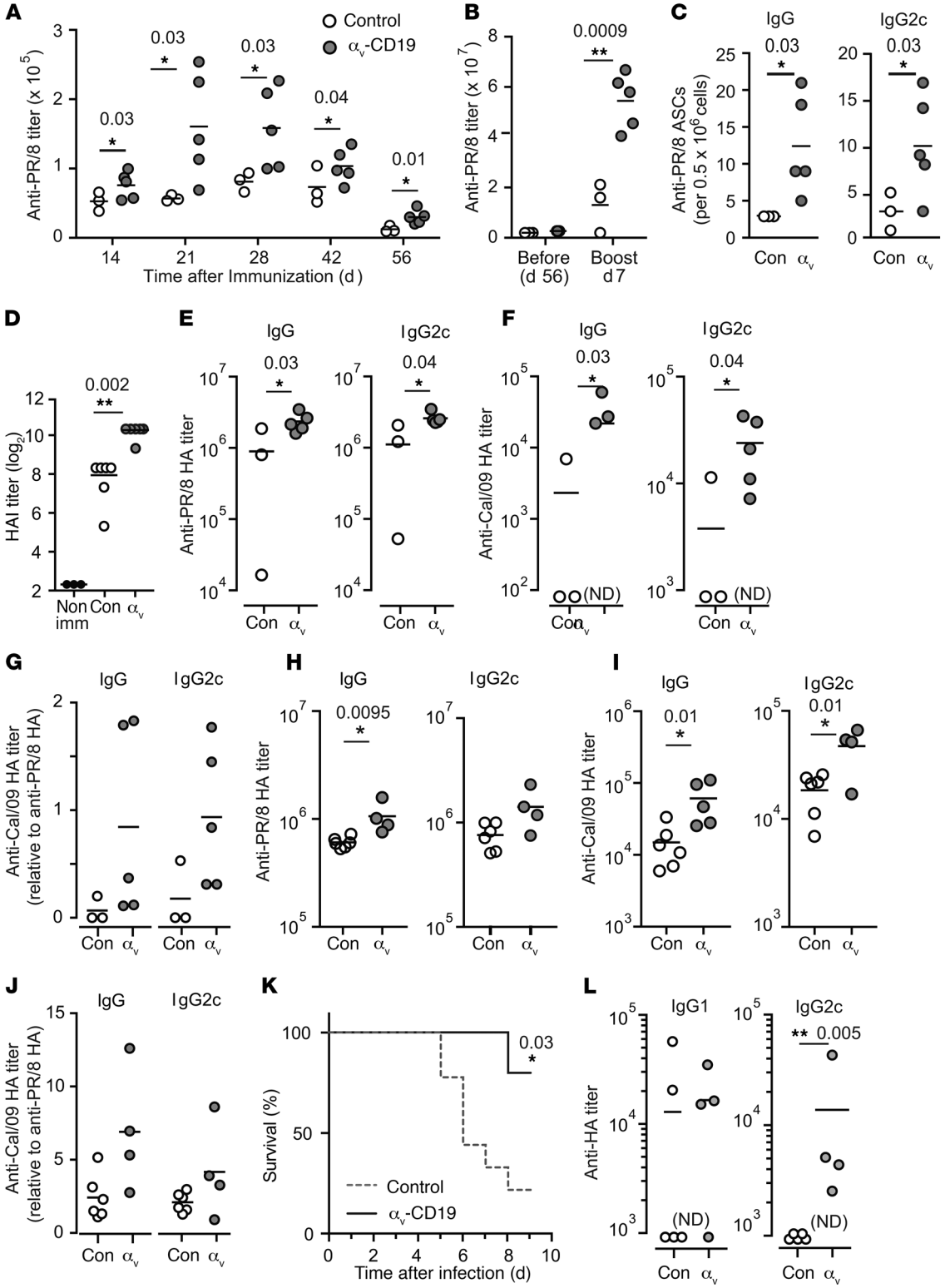

Figure 9. Deletion of α_v enhances antibody response to influenza virus. (**A** and **B**) Serum anti-PR/8 IgG titers in control and α_v-CD19 mice immunized with 10 μg of inactivated H1N1 PR/8 (**A**) and (**B**) boosted at day 57 with 5 μg inactivated PR/8. (**C**) PR/8-specific plasma cells enumerated by ELISpot in BM cells from control (Con) and α_v-CD19 mice harvested at day 7 after boost. (**D**) HAI activity in sera from control and α_v-CD19 mice at day 21 after PR/8 immunization. (**E** and **F**) Serum antibody titers against HA from H1N1 PR/8 (**E**) or H1N1 Cal/09 (**F**) in control and α_v-CD19 mice at day 7 after boost with inactivated PR/8. (**G**) Anti-Cal/09 HA titer normalized to anti-PR/8 HA titer. (**H** and **I**) Serum antibody titers against HA from PR/8 (**H**) or Cal/09 (**I**) in control and α_v-CD19 at day 51 after immunization with inactivated PR/8 (10 μg) in imiquimod-SE (10 μg). (**J**) Anti-Cal/09 HA titer normalized to anti-PR/8 HA titer for mice immunized with PR/8 in imiquimod-SE. (**K**) Survival of control and α_v-CD19 mice following intranasal infection with PR/8 ($n \geq 5$ mice/group). (**L**) Anti-PR8 HA titers from surviving mice at day 7 after infection. All data points represent individual mice with mean shown. *P* values of less than 0.05 are shown (Mann-Whitney-Wilcoxon test for antibody titers or Mantel-Cox test for survival curves).*$P < 0.05$; **$P < 0.005$. Samples below the level of detection are indicated as not detected. For all data, similar results were seen in at least 3 independent experiments.

with studies showing that TLR ligand adjuvants can increase the breadth of anti-HA reactivity during influenza vaccination (22–24), control mice consistently produced Cal/09-HA crossreactive antibody (Figure 9I). However, even in the presence of this strong adjuvant, α_v-CD19 mice produced higher levels of anti-PR/8 and anti-Cal/09 HA antibodies (Figure 9, H and I) and an increase in the ratio of Cal/09 to PR/8 HA binding (Figure 9J), as seen with immunization without adjuvant. Hence, together, these data demonstrate that deletion of α_v from B cells causes increased functional antibody responses to immunization with inactivated virus and, moreover, that this response is of greater breadth than in control mice.

The accelerated and increased antibody response to inactivated PR/8 suggested to us that α_v-CD19 mice may be protected from viral infection. To test this, we infected α_v-CD19 mice and littermate control mice with live PR/8. As shown in Figure 9K, the majority of control mice had to be euthanized during the course of infection due to excessive weight loss or other pathology. In contrast, almost all α_v-CD19 mice survived infection and regained any weight loss by 8 to 9 days after infection. Supporting a role for increased antibody responses in increased protection, α_v-CD19 mice had clearly detectable levels of class-switched IgG2c anti-HA antibody 7 days after infection, whereas these antibodies were undetectable in surviving control mice at the same time point (Figure 9L). Titers of IgG1 were observed in both α_v-CD19 mice and controls.

Discussion

Although the role of B cell TLRs in promoting effective immunity is increasingly appreciated, the factors that affect TLR signaling in these cells and how these affect immune responses remain poorly understood. Here, we describe a mechanism of regulation of TLR signaling in GC B cells mediated by α_v integrins. We show that disruption of this regulatory mechanism by deletion of α_v in B cells enhances responses to antigens containing TLR ligands and influenza virus, causing increases in GC B cell expansion, affinity maturation, and class switching to IgG2c and promoting generation of memory and plasma B cells. Our results establish the concept that increasing TLR signaling in B cells is sufficient for promoting GC B cell development and differentiation, leading to stronger, high-affinity, long-lived antibody responses that are relevant for response to viruses. Furthermore, we show that this α_v-mediated regulatory pathway is associated with GC B cell–specific activation of the autophagy protein LC3, identifying a potential new regulatory role for autophagy components in GC B cells.

Previous studies using genetic targeting of individual TLRs or the TLR-signaling adaptor Myd88 have shown that disruption of TLR signaling in B cells causes loss of class switching, affinity maturation, and generation of memory cells (4, 18). Our findings that α_v deletion in B cells increases these responses are therefore consistent with effects on B cell TLR signaling. Furthermore, our data provide an important complement to these earlier studies, establishing that increased TLR signaling in GC cells alone is sufficient to increase immune responses. The ability of GC B cells to signal though TLRs is thought to be particularly important in antiviral immunity, allowing vigorous responses to viral nucleic acids (18, 25, 26). In this context, it is curious that a number of viruses bind $\alpha_v\beta_3$ directly to promote their internalization, and $\alpha_v\beta_3$ has been proposed to function as an innate immune receptor for herpes simplex virus (27). It is therefore possible that the α_v autophagy pathway that we describe is activated by viral engagement of $\alpha_v\beta_3$ and plays an important role in antiviral immunity. This is an active ongoing area of study. However, $\alpha_v\beta_3$ also serves as a phagocytic receptor for apoptotic cells and cellular debris (28, 29), which are known sources of self-antigen that can promote autoimmune disease. We showed previously that deletion of α_v from B cells results in the expansion of autoreactive MZ and B-1 B cells and that α_v-CD19 mice have higher titers of autoreactive natural antibodies and autoantibodies to dsDNA (10). We therefore hypothesize that a major role for the α_v autophagy pathway is to regulate responses to self-derived nucleic acids and other TLR ligands, limiting B cell TLR signaling to prevent generation of high-affinity, class-switched antibodies from apoptotic material internalized through α_v integrins. Here, we show that this mechanism of autoimmune regulation also affects potentially protective responses to foreign antigens and that release of this regulatory mechanism enhances generation of high-affinity IgG2c antibodies to TLR-associated antigens through effects on GC B cells.

Based on the effects of α_v deletion on TLR-signaling pathways and TLR-dependent functions, we conclude that the phenotype of α_v-CD19 mice is primarily due to loss of regulation of TLR signaling. Furthermore, based on the high expression of $\alpha_v\beta_3$ in GC B cells and the observation that $\beta3^{-/-}$ B cells also show increased TLR signaling (10), it is likely that $\alpha_v\beta_3$ is the integrin heterodimer responsible. β_3 has previously been implicated in GC B function, and B cell–specific $\beta3^{-/-}$ mice (generated by BM chimera) also show increased numbers of spontaneous intestinal GC cells, closely mirroring our results (16). In this previous study, the authors speculated that $\alpha_v\beta_3$ may mediate adhesion or migration of GC B cells. Although we cannot exclude contributions of α_v integrins in GC B cell migration (as has been shown for T cells; refs. 30, 31) or other roles, such as activation of TGF-β (30, 32), the lack of effect of α_v deletion on B cell responses to immunization with the TLR-independent adjuvant alum strongly argues for our proposed role for α_v in TLR signaling and against a critical role for these integrins in other functions of B cells.

$\alpha_v\beta_3$ Regulates TLR signaling by activating lipidation of the autophagy component LC3b and promoting recruitment of LC3b to TLR-containing endosomes (10). LC3b recruitment initially allows TLRs to signal via IRF7, but subsequently promotes the fusion of TLR-containing endosomes with the lysosome, terminating signaling. As we show here, deletion of α_v severely inhibits this process in GC B cells, resulting in increased and prolonged TLR signaling. Although this process involves components of the autophagy machinery, we do not believe it constitutes "canonical" autophagy (also termed macroautophagy), as we see no evidence of the formation of archetypal double-membrane autophagosomes (10); instead, the involvement of Rubicon in this process indicates that it occurs through a noncanonical pathway, which is similar to the involvement of LC3 in phagocytosis (15, 19). Signaling in non-GC follicular B cells does not appear to be regulated by this α_v autophagy mechanism, and expression of $\alpha_v\beta_3$, LC3, and p62 are all reduced or absent in these cells. Therefore, the ability to activate this α_v autophagy regulatory pathway appears to be acquired by B cells as they differentiate in the GC and upregulate

TLR signaling machinery. A recent study showed that GC B cells switch from canonical to noncanonical pathways of autophagy activation during viral infection, although the outcome of this change was unclear (33). Our data are in agreement with this and provide insight into the role for noncanonical autophagy in directing TLR signaling to IRF7 and promoting delivery of internalized ligands to lysosomes (which may promote IRF7 signaling/IFN production and antigen presentation, respectively).

Although we focus here on the effects on TLR signaling, it is likely that α_v-mediated noncanonical autophagy has additional roles in GC B cells, such as antigen presentation, as has been proposed for LC3-associated autophagy. Both canonical and noncanonical autophagy are involved in many other processes in B cells, including responding to increased energy demands during rapid cell division or unfolded protein responses during antibody production. Disruption of autophagy components required for both canonical and noncanonical autophagy in B cells results in more severe phenotypes than we see in α_v-CD19 mice, including marked defects in memory and plasma cell responses (34, 35). Dissecting these complex roles for the fundamental process of autophagy will therefore require further identification and study of specific activators of the autophagy machinery, such as α_v.

The induction of memory B cells and long-lived plasma cells by vaccines is central for their ability to provide long-term protection (36, 37). Furthermore, promoting B cell SHM to generate antibodies with greater affinity or breadth is critical for generating effective immunity to pathogens, such as viruses, that have the capacity to mutate rapidly. This is of particular importance in generating effective neutralizing antibodies to viruses, as emerging evidence from studies of HIV and influenza suggest that effective neutralizing antibodies can require a large number of mutations and potentially several rounds of affinity maturation in the GC. We show here that modulating TLR signaling through the α_v autophagy pathway can promote mutations in antibody sequences in GC B cells, increasing antibody affinity, as well as enhance the generation of long-lived plasma cell response against both VLPs and intact influenza virus. In addition, our results show that increased SHM due to loss of α_v on B cells could be effective in generating crossreactive antibodies against different HA subtypes, and we are investigating this in more detail in ongoing studies. TLR ligands have already been harnessed as vaccine adjuvants and are important for immune responses to inactivated or attenuated vaccines (38, 39). Our data suggest that inhibition of regulatory pathways for TLR signaling, such as $\alpha_v\beta_3$, would enhance their effectiveness, an attractive prospect, as selective agonists and antagonists for α_v integrins, such as cilengitide or antibodies, have been developed and used clinically in other settings (40, 41). In summary, we have identified a mechanism of regulation of GC B cell response by α_v integrins and autophagy proteins and this work, together with other recent studies, points to B cell TLR signaling as an important and distinct target for promoting high-affinity long-lived antibody responses to viral antigens.

Methods

Mice. α_v-CD19 were generated as previously described (10) and maintained on a mixed C57BL/6/129 Ola background. Littermates with a single *Cd19-Cre* allele and *Itgav*-flox alleles were used as controls. As the background strains of these mice differ at their Igh-1 loci and in their ability to make IgG2a versus IgG2c (42), for immunization experiments, mice were matched by Igh-1 genotype (all were Igh-1 a/b). α_v-CD19 mice backcrossed to a C57BL/6 background (10 generations) were used for all influenza immunization and challenge experiments. C57BL/6-background α_v-CD19 mice were intercrossed with C57BL/6. SJL congenic mice for generation of BM chimeras. Rubicon-KO mice on a C57BL/6 background (19) were obtained from Jennifer Martinez (National Institute of Environmental Health Sciences, Durham, North Carolina, USA). Both male and female mice of 8 to 12 weeks of age were used for experiments. All mice were housed under specific pathogen–free conditions at Benaroya Research Institute. μMT mice were bred and maintained at Seattle Children's Research Institute animal facility under specific pathogen–free conditions.

Antibodies and reagents. Anti-mouse antibodies used for flow cytometry included the following. CD95 (Jo2/BV421, catalog 562633; PE, catalog 554258), CD138 (281-2/BV421, catalog 562610), CD4 (RM4-5/BV510, catalog 563106), CXCR4 (2B11/CXCR4/BV421, catalog 562738) CD38 (90/Percp-CY5.5, catalog 562770), B220 (RA3-6B2/PE-CY7, catalog 552772), CD11b (M1/70/PE, catalog 557397), IgM (R6-60.2/PE, catalog 553409; BV510, catalog 747733), IgD (11-26c.2a/BV605, catalog 563003), CD19 (1D3/BV650, catalog 563235; APC-CY7, catalog 557655; PE-CY7, catalog 552854), CD23 (B3B4, PE-CY7, catalog 562825), and mouse BD Fc block (2.4G2,catalog 553142) were from BD Biosciences. GL7 (GL7/efluor 660, catalog 50-5902-82) and anti-integrin α_v antibody (ebioHMA5-1, catalog 11-0493-81) were from eBioscience. CD86 (GL1, Percp-CY5.5, catalog 105028) and CD73 (Ty/11.8, Perp-CY5.5, catalog 127213) were from BioLegend. Goat anti-rabbit IgG (H+L) Alexa Fluor 546 (catalog A11010), streptavidin Alexa Fluor 647 (catalog s32357), and Hoechst 33342 were from Invitrogen (Molecular Probes). Type C -CpG-ODN 2395, Type B CpG ODN 1826, and imiquimod were from Invivogen. Antibodies to anti–NF-κB p65 (D14E12, catalog 8242), anti-LSD1 (C69G12,catalog 2184), and horseradish peroxidase–conjugated anti-rabbit IgG were from Cell Signaling Technology. Anti-LC3B anti–β-actin (AC-15, catalog L7543) and LPS (from *E. coli* O55:B5) were from Sigma-Aldrich. Alkaline phosphatase–conjugated anti-mouse IgG-AP (catalog 1030-04), anti-mouse IgG2c-AP (catalog 1079-04), anti-mouse IgG1-AP (catalog 1070-04), anti-mouse IgM-AP (catalog 1020-04), and anti-mouse IgG(H+L) (catalog 1010-01) were from Southern Biotech. PNA-FITC was from Vector Laboratories. P62 antibody (catalog 03GP62-C) was from American Research Products. IRF antibody was from Santa Cruz Biotechnology Inc. (H-246, catalog sc9083). Recombinant HA from PR8 or Cal/09 was purchased from Sino Biological. H1N1 PR/8 was purchased from Charles River Laboratories. Vaccine-grade TLR7 ligand adjuvant imiquimod-SE was from the Infectious Disease Research Institute.

Flow cytometry and cell sorting. Cells were harvested in PBS/0.5% BSA/ 2 mM EDTA, and splenocytes or BM cells were depleted of red blood cells (ACK Lysis Buffer; Gibco, Thermo Fisher Scientific). Single-cell suspensions were blocked with Fc Block (BD Biosciences) and stained with fluorochrome-tagged antibodies for surface markers (1:200 dilution) at 4°C for 30 minutes. For detection of Qβ-specific cells, cells were stained with Alexa Fluor 647–labeled Qβ-VLPs together with the antibodies for surface markers. Samples were acquired using an LSRII flow cytometer (BD) and analyzed by FlowJo software (Tree Star Inc.). For sorting of spleen GC and follicular cells, after B cell enrichment with the negative selection cocktail (Stem Cell Technol-

ogies), cells were labeled with anti–B220-PE-CY7, anti–CD38-PerCP-CY5.5, anti–CD95-BV421, and anti–PNA-FITC antibodies, then sorted with FACS Aria (BD Bioscience).

In vitro proliferation. FACS-sorted spleen MZ and follicular or peritoneal cavity B1 cells were plated in X-VIVO15 (Lonza) supplemented with 2 mM glutamine, 100 U/ml penicillin, and 100 μg/ml streptomycin and 50 μM 2-β-mercaptoethanol or complete RPMI-1640 (10% FBS, 2 mM glutamine, 100 U/ml penicillin and 100 μg/ml streptomycin, and 50 μM 2-β-mercaptoethanol) at a density of 3×10^4 cells per well on a 96-well plate and treated with different stimuli: CpG (2 μM), immiquimod (10 μM), and IgM (10 μg/ml). After 48 hours, cells were pulsed with 1 μCi/well tritiated thymidine ([3H]-TdR) for 18 hours prior to harvest; incorporation was determined by liquid scintillation spectrometry.

In vivo proliferation. Mice were injected with 2 μg VLPs i.p., and 12 hours before harvest on day 14, were injected i.p with 1 mg BrdU (BD Biosciences). Cells were then harvested from spleen and lymph nodes and stained for surface antigen as described and processed using an anti–BrdU-FITC kit (BD Biosciences).

BCR sequencing. Single VLP$^+$ GC (CD19$^+$VLP$^+$PNA$^+$FAS$^+$CD38$^-$) cells were FACS sorted into a 96-well plate using Aria II. BCRs were amplified and sequenced from cDNA of single cells as previously described (20, 43). The numbers of SHM in both heavy- (V_H) and light-chain (V_L) sequences in individual cells were calculated after comparison with germline sequence.

BM transplantations. BM was harvested from femora and tibiae of C57BL/6.SJL (control with CD45.1 congenic marker), α_v-CD19 (CD45.2 congenic marker), and C57BL/6 (control with CD45.2 congenic marker) mice. Single-cell suspensions were CD138 depleted (Miltenyi Biotech) and mixed at a 50:50 ratio (control CD45.1: α_v-CD19 CD45.2 or control CD45.1: control 45.2), and 6×10^6 Total BM was injected into lethally irradiated (450cGY X2 doses) μ-MT recipients. The resulting chimeras were bled at 4 weeks to check chimerism in blood and at 6 weeks were immunized with 2 μg VLP. Spleen and lymph nodes were harvested for analysis at day 14 after immunization.

Confocal microscopy. FACS-sorted GC B cells or non-GC follicular cells were seeded onto poly-L-lysine–coated glass coverslips (BD BioCoat) in complete RPMI 1640 and allowed to attach for 1 hour at 37°C. Cells were stimulated with 3 μM CpG or 1 μg/ml VLPs for the indicated times. After stimulation, cells were fixed with 4% PFA for 20 minutes at room temperature (RT) and permeabilized with saponin (0.2% saponin in PBS, 0.03 M sucrose, 1% BSA) for 10 minutes at RT. Nonspecific binding in cells was prevented by incubating for 1 hour at RT with blocking buffer (2% goat serum, 1% BSA, 0.1% cold fish skin gelatin, 0.1% saponin, 0.05% Tween-20 in 0.01 M PBS, pH 7.2). Cells were incubated overnight at 4°C with primary antibody (LC3, 1:500 dilution) in dilution buffer (PBS, 0.05% Tween-20, 1% BSA, 0.1% saponin). Cells were washed 3 times in dilution buffer (5 minutes each time), incubated in secondary antibodies (1: 500 dilution) in dilution buffer for 1 hour at RT, and washed 3 times in dilution buffer and twice in PBS. Cell nuclei were stained with Hoechst 33342, and the coverslips were mounted with ProLong Antifade (Invitrogen). Cells were imaged in a ×100 oil objective (aperture 1.4) and Nikon Ti (Eclipse) inverted microscope with an Ultraview Spinning Disc (CSU-X1) confocal scanner (PerkinElmer). Images were captured with an Orca-ER Camera using Volocity (PerkinElmer). Postacquisition analysis, such as contrast adjustment, deconvolution through iterative restoration, and 3D reconstruction, were performed using Volocity software. LC3 puncta were quantified by counting 10 to 50 cells per condition in a blinded manner and defining LC3-staining patterns as distributed around the cells or as punctate.

ELISA. Immulon 2HB microtiter plates (DYNEX) were coated with either NP-BSA (Biosearch Technologies) (10 μg/ml), VLPs (2 μg/ml), inactivated PR/8 (1 μg/ml), or recombinant HA from PR/8 or HA from Cal/09 (0.5 μg/ml) in PBS overnight at 4°C. Plates were then washed and blocked for 60 minutes at 37°C (2% BSA, 2% FCS, 0.1% Tween-20, 0.02% sodium azide in PBS). Serum samples were initially diluted at 1:200 in 50% block and then loaded onto the plate as a 6-point series of 4-fold dilutions. After incubation for 60 to 120 minutes at 37°C, bound antibody was detected using alkaline phosphatase–conjugated goat anti-mouse IgM or IgG (Southern Biotech) diluted in blocking buffer for 60 minutes at 37°C. Secondary antibodies were detected by using disodium p-nitrophenyl phosphate substrate (Sigma-Aldrich) and absorbance (OD) read at 405 nm. Antibody titers were calculated from comparisons of dilutions required to achieve the same OD relative to a standard antibody.

ELISpot. To detect antigen-specific long-lived plasma cells in the BM, 96-well filter plates (Millipore) were coated overnight with antigen: 2 μg/ml VLP, 10 μg/ml NP-BSA in PBS at 4°C. After blocking with RPMI 1640 with 10% FBS for 1 hour, 2-fold dilutions of BM single-cell suspension were added to the filter plates starting with 2×10^6 cells/well in RPMI 1640 with 10% FBS and incubated for 12 hours at 37°C. Plates were washed with PBS and incubated with AP-conjugated anti-mouse IgM, total IgG, IgG1, or IgG2c (Southern Biotechnology) and developed with BCIP/NBT alkaline phosphate substrate kit (Vector Laboratories). Plates were washed with water and positive cells were counted in each well.

Western blots. Nuclear extracts were prepared by lysing cells in hypotonic nuclear extraction buffer (1 M HEPES, pH 7.5, 5 M NaCl, 0.5 M EDTA pH 8, 50% glycerol, 10% igepal, 10% Triton X-100) for 10 minutes, followed by centrifugation at 1,500 *g* for 5 minutes at 4°C to pellet the nuclei, and nuclei were resuspended in RIPA buffer. Lysates were centrifuged for 10 minutes at 4°C at 14,000 *g*, and supernatant was collected as nuclear fraction. Proteins were quantified by BCA assay (Pierce), separated by electrophoresis using NuPage-Bis-Tris gels (Invitrogen), and blotted onto PVDF membranes. Nonspecific binding was blocked with 5% BSA in TBS-Tween (0.1%), followed by incubation with primary antibodies (1:1000 dilution) overnight at 4°C and secondary antibody horseradish peroxidase–conjugated antibodies (1:2,000 dilution) for 1 hour at RT. Membranes were washed thoroughly with TBS-Tween (0.1%) after antibody incubations and developed using ECL reagents (Millipore). For reprobing, blots were stripped for 30 minutes at 37°C with Restore PLUS Stripping Buffer (Thermo Scientific).

Immunizations/infection. For experiments using TLR ligands and alum as adjuvants, mice were immunized i.p. with NP-haptenated chicken γ globulin (NP-CG) (Biosearch Technologies), 50 μg per mouse in combination with alum (1:1) or LPS (5 μg /mouse) or clinical grade TLR7 ligand adjuvant imiquimod-SE (Infectious Disease Research Institute). For VLP experiments, VLP derived from Qβ bacteriophages were provided by Baidong Hou (Institute of Biophysics, Chinese Academy of Sciences, Beijing, China). The production of these particles has been described previously (18). Mice were immunized i.p. with 2 μg VLPs, and serum was collected at indicated time points by submandibular bleeds. For studies with intact virus, mice were immunized i.p.

with 10 μg inactivated H1N1 PR/8 influenza virus (Charles River Laboratories). For challenge studies, mice were infected intranasally with 1XLD50 H1N1 PR/8 (Charles River Laboratories) diluted in 25 μl PBS.

qPCRs. RNA was isolated from VLP$^+$ GC cells (CD19$^+$ VLP$^+$PNA$^+$FAS$^+$) or total VLP$^+$ B cells FACS sorted directly into TRIzol-LS (Invitrogen) and converted into cDNA by reverse transcription (Applied Biosystems). Real-time PCR was performed with SYBR Green using the following primers: *Aicda*, 5′-CCTCCTGCTCACTGGACTTC-3′ (forward) and 5′-GGCTGAGGTTAGGGTTCCAT-3′ (reverse); *Tbx-21*,5′-GGTGTCTGGGAAGCTGAGAG-3′ (forward) and 5′-CCACATCCACAAACATCCTG-3′ (reverse); *Bcl6*,5′-TCGTGAGGTCGTGGAGAAC-3′ (forward) and 5′-AGAGAAGAGGAAGGTGCTGAG-3′ (reverse); *Prdm1*, 5′-TGCGGAGAGGCTCCACTA-3′ (forward) and 5′-TGGGTTGCTTTCCGTTTG-3′ (reverse); *Myc*, 5′-TCTCCACTCACCAGCACAACTACG-3′ (forward) and 5′-ATCTGCTTCAGGACCCT-3′ (reverse); and *Actb*, 5′-GCCCATCTACGAGGGCTATG-3′ (forward) and 5′-CTCAGCTGTGGTGGTGAAGC-3′ (reverse),

Statistics. All statistical tests used are indicated in the relevant figure legends. Statistical analysis was performed using GraphPad Prism, using multiple testing corrections where appropriate. A *P* value of less than 0.05 was considered significant.

Study approval. All animal experiments were approved following institutional review by the Animal Care and Use Committees at Benaroya Research Institute and Seattle Children's Hospital Research Institute. Experiments were performed under local and national guidelines for animal care.

Author contributions

FR and MA designed and performed experiments. Additional expertise and assistance in experimental design, execution, and analysis were provided by SS, TA, GM, SD, SWJ, and DJR (BM chimeras and BCR sequencing). MTO and EG provided reagents and advised on immunization and influenza infection experiments. MA, ALH, and LMS designed and conceived the study and wrote the paper.

Acknowledgments

We thank all members of the Acharya, Lacy-Hulbert, Stuart, and Rawlings labs for assistance and advice on this project. This work was supported by NIH grant DK093695 (to ALH).

Address correspondence to: Lynda Stuart, Bill and Melinda Gates Foundation, 500 Fifth Avenue, Seattle, Washington 98109, USA. Phone: 206.245.9468; Email: Lynda.stuart@gatesfoundation.org. Or to: Mridu Acharya, Benaroya Research Institute at Virginia Mason, 1201 Ninth Avenue, Seattle, Washington 98101, USA. Phone: 206.341.8997; Email: macharya@benaroyaresearch.org.

1. Victora GD, Nussenzweig MC. Germinal centers. *Annu Rev Immunol*. 2012;30:429–457.
2. Bannard O, Cyster JG. Germinal centers: programmed for affinity maturation and antibody diversification. *Curr Opin Immunol*. 2017;45:21–30.
3. DeFranco AL. The germinal center antibody response in health and disease. *F1000Res*. 2016;5:F1000.
4. Rookhuizen DC, DeFranco AL. Toll-like receptor 9 signaling acts on multiple elements of the germinal center to enhance antibody responses. *Proc Natl Acad Sci U S A*. 2014;111(31):E3224–E3233.
5. Kasturi SP, et al. Programming the magnitude and persistence of antibody responses with innate immunity. *Nature*. 2011;470(7335):543–547.
6. DeFranco AL, Rookhuizen DC, Hou B. Contribution of Toll-like receptor signaling to germinal center antibody responses. *Immunol Rev*. 2012;247(1):64–72.
7. Leadbetter EA, Rifkin IR, Hohlbaum AM, Beaudette BC, Shlomchik MJ, Marshak-Rothstein A. Chromatin-IgG complexes activate B cells by dual engagement of IgM and Toll-like receptors. *Nature*. 2002;416(6881):603–607.
8. Teichmann LL, Schenten D, Medzhitov R, Kashgarian M, Shlomchik MJ. Signals via the adaptor MyD88 in B cells and DCs make distinct and synergistic contributions to immune activation and tissue damage in lupus. *Immunity*. 2013;38(3):528–540.
9. Jackson SW, et al. Opposing impact of B cell-intrinsic TLR7 and TLR9 signals on autoantibody repertoire and systemic inflammation. *J Immunol*. 2014;192(10):4525–4532.
10. Acharya M, et al. α_v Integrins combine with LC3 and atg5 to regulate Toll-like receptor signalling in B cells. *Nat Commun*. 2016;7:10917.
11. Barton GM, Kagan JC. A cell biological view of Toll-like receptor function: regulation through compartmentalization. *Nat Rev Immunol*. 2009;9(8):535–542.
12. Kagan JC, Su T, Horng T, Chow A, Akira S, Medzhitov R. TRAM couples endocytosis of Toll-like receptor 4 to the induction of interferon-beta. *Nat Immunol*. 2008;9(4):361–368.
13. Husebye H, et al. Endocytic pathways regulate Toll-like receptor 4 signaling and link innate and adaptive immunity. *EMBO J*. 2006;25(4):683–692.
14. Sasai M, Linehan MM, Iwasaki A. Bifurcation of Toll-like receptor 9 signaling by adaptor protein 3. *Science*. 2010;329(5998):1530–1534.
15. Sanjuan MA, et al. Toll-like receptor signalling in macrophages links the autophagy pathway to phagocytosis. *Nature*. 2007;450(7173):1253–1257.
16. Wang X, Rodda LB, Bannard O, Cyster JG. Integrin-mediated interactions between B cells and follicular dendritic cells influence germinal center B cell fitness. *J Immunol*. 2014;192(10):4601–4609.
17. Jegerlehner A, Maurer P, Bessa J, Hinton HJ, Kopf M, Bachmann MF. TLR9 signaling in B cells determines class switch recombination to IgG2a. *J Immunol*. 2007;178(4):2415–2420.
18. Hou B, et al. Selective utilization of Toll-like receptor and MyD88 signaling in B cells for enhancement of the antiviral germinal center response. *Immunity*. 2011;34(3):375–384.
19. Martinez J, et al. Molecular characterization of LC3-associated phagocytosis reveals distinct roles for Rubicon, NOX2 and autophagy proteins. *Nat Cell Biol*. 2015;17(7):893–906.
20. Tiller T, Busse CE, Wardemann H. Cloning and expression of murine Ig genes from single B cells. *J Immunol Methods*. 2009;350(1–2):183–193.
21. Pappas L, et al. Rapid development of broadly influenza neutralizing antibodies through redundant mutations. *Nature*. 2014;516(7531):418–422.
22. Clegg CH, et al. Adjuvant solution for pandemic influenza vaccine production. *Proc Natl Acad Sci U S A*. 2012;109(43):17585–17590.
23. Goff PH, et al. Synthetic Toll-like receptor 4 (TLR4) and TLR7 ligands as influenza virus vaccine adjuvants induce rapid, sustained, and broadly protective responses. *J Virol*. 2015;89(6):3221–3235.
24. Van Hoeven N, et al. A formulated TLR7/8 agonist is a flexible, highly potent and effective adjuvant for pandemic influenza vaccines. *Sci Rep*. 2017;7:46426.
25. Browne EP. Toll-like receptor 7 controls the anti-retroviral germinal center response. *PLoS Pathog*. 2011;7(10):e1002293.
26. Clingan JM, Matloubian M. B cell-intrinsic TLR7 signaling is required for optimal B cell responses during chronic viral infection. *J Immunol*. 2013;191(2):810–818.
27. Gianni T, Leoni V, Chesnokova LS, Hutt-Fletcher LM, Campadelli-Fiume G. αvβ3-integrin is a major sensor and activator of innate immunity to herpes simplex virus-1. *Proc Natl Acad Sci U S A*. 2012;109(48):19792–19797.
28. Lucas M, et al. Requirements for apoptotic cell contact in regulation of macrophage responses. *J Immunol*. 2006;177(6):4047–4054.
29. Savill J, Dransfield I, Hogg N, Haslett C. Vitronectin receptor-mediated phagocytosis of cells undergoing apoptosis. *Nature*. 1990;343(6254):170–173.
30. Lacy-Hulbert A, et al. Beta 3 Integrins regulate lymphocyte migration and cytokine responses in heart transplant rejection. *Am J Transplant*. 2007;7(5):1080–1090.

31. Overstreet MG, et al. Inflammation-induced interstitial migration of effector CD4+ T cells is dependent on Integrin αV. *Nat Immunol*. 2013;14(9):949–958.
32. Acharya M, et al. α_v Integrin expression by DCs is required for Th17 cell differentiation and development of experimental autoimmune encephalomyelitis in mice. *J Clin Invest*. 2010;120(12):4445–4452.
33. Martinez-Martin N, et al. A switch from canonical to noncanonical autophagy shapes B cell responses. *Science*. 2017;355(6325):641–647.
34. Chen M, et al. Essential role for autophagy in the maintenance of immunological memory against influenza infection. *Nat Med*. 2014;20(5):503–510.
35. Pengo N, et al. Plasma cells require autophagy for sustainable immunoglobulin production. *Nat Immunol*. 2013;14(3):298–305.
36. Ahmed R, Gray D. Immunological memory and protective immunity: understanding their relation. *Science*. 1996;272(5258):54–60.
37. Pulendran B, Ahmed R. Translating innate immunity into immunological memory: implications for vaccine development. *Cell*. 2006;124(4):849–863.
38. Querec T, et al. Yellow fever vaccine YF-17D activates multiple dendritic cell subsets via TLR2, 7, 8, and 9 to stimulate polyvalent immunity. *J Exp Med*. 2006;203(2):413–424.
39. Reed SG, Orr MT, Fox CB. Key roles of adjuvants in modern vaccines. *Nat Med*. 2013;19(12):1597–1608.
40. Desgrosellier JS, Cheresh DA. Integrins in cancer: biological implications and therapeutic opportunities. *Nat Rev Cancer*. 2010;10(1):9–22.
41. Byron A, Humphries JD, Askari JA, Craig SE, Mould AP, Humphries MJ. Anti-integrin monoclonal antibodies. *J Cell Sci*. 2009;122(pt 22):4009–4011.
42. Zhang Z, Goldschmidt T, Salter H. Possible allelic structure of IgG2a and IgG2c in mice. *Mol Immunol*. 2012;50(3):169–171.
43. Schwartz MA, Kolhatkar NS, Thouvenel C, Khim S, Rawlings DJ. CD4+ T cells and CD40 participate in selection and homeostasis of peripheral B cells. *J Immunol*. 2014;193(7):3492–3502.